ARTICLE

Fabrication of Buckling Free Ultrathin Silicon Membranes by Direct Bonding with Thermal Difference

Florian Delachat,[*,†,‡] Christophe Constancias,[‡] Frank Fournel,[‡] Christophe Morales,[‡] Boris Le Drogoff,[§] Mohamed Chaker,[§] and Joelle Margot[†]

[†]Université de Montréal, C.P. 6128, Montréal, Québec H3C 3J7, Canada, [‡]CEA-LETI, 17 rue des Martyrs, Grenoble F-38054, France, and [§]INRS-EMT, 1650 Boulevard Lionel-Boulet, Varennes, Québec J3X 1S2, Canada

ABSTRACT An innovative method to fabricate large area (up to several squared millimeters) ultrathin (100 nm) monocrystalline silicon (Si) membranes is described. This process is based on the direct bonding of a silicon-on-insulator wafer with a preperforated silicon wafer. The stress generated by the thermal difference applied during the bonding process is exploited to produce buckling free silicon nanomembranes of large areas. The thermal differences required to achieve these membranes ($\geq$1 mm^2) are estimated by analytical calculations. An experimental study of the stress achievable by direct bonding through two specific surface preparations (hydrophobic or hydrophilic) is reported. Buckling free silicon nanomembranes secured on a 2 $\times$ 2 cm^2 frame with lateral dimensions up to 5 $\times$ 5 mm^2 are successfully fabricated using the optimized direct bonding process. The stress estimated by theoretical analysis is confirmed by Raman measurements, while the flatness of the nanomembranes is demonstrated by optical interferometry. The successful fabrications of high resolution (50 nm half pitch) tungsten gratings on the silicon nanomembranes and of focused ion beam milling nanostructures show the promising potential of the Si membranes for X-ray optics and for the emerging nanosensor market.

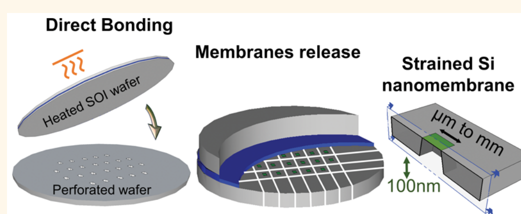

KEYWORDS: nanotechnology · direct bonding · silicon · nanomembranes · nanofabrication

Ultrathin membranes are currently very attractive for a wide variety of applications in the field of physics, optics and biology,[1] while silicon is extensively used in microelectronics and in micro/nanoelectro-mechanical systems. Therefore, producing nanostructured, highly reproducible ultrathin silicon membranes at a relatively moderate cost would be a major asset for several applications including nanosensors,[2] nanoperforated membranes for efficient separation of nanoparticles or biological materials[3,4] and nanopatterned membranes for optical applications.[5] Silicon (Si) also enables a facilitated integration for devices that combine microfluidics, electronics and sensors.[6,7]

The conventional method to fabricate Si nanomembranes is to etch the backside of a bonded silicon-on-insulator (SOI) wafer through the Si wafer in order to release the top Si layer using the buried oxide layer as a convenient etch stop layer. However, the oxide/silicon interface induces a compressive stress of several tens of MPa,[8] which irremediably results in the detrimental buckling of the membrane for numerous applications. Further removing of the buried oxide on the membranes does not solve completely this issue. Indeed the oxide generates rippled membranes due to the stress released at the edge of the membrane.[9,10] In the scientific literature, several strategies have been proposed to engineer the Si film strain in order to avoid bending after membrane release. An elegant method consists in adjusting the stress in the Si layer with the use of elastically strained layers which transfer their energy to the Si layer.[11] The stressed heterostructure releases its strain elastically by lateral expanding. As a result, the Si membrane is stretched. This strategy results in transferrable Si/Ge sheets that are very appealing for photonics (*e.g.*, band gap engineering based applications).[12] However, for biological or optic purposes, the Si/Ge multilayer is not appropriate, mainly because the membrane should be held by a frame

* Address correspondence to florian.delachat@umontreal.ca.

Received for review September 12, 2014 and accepted March 19, 2015.

Published online March 19, 2015
10.1021/acsnano.5b00234

© 2015 American Chemical Society

and because of its unfavorable heterostructure properties. An alternative has been published recently by Shchepetov *et al.*[10] They proposed the use of a strain compensating frame of silicon nitride on the silicon perimeter. Appropriate tuning of the silicon nitride properties enables one to avoid membrane buckling. Furthermore, it is also possible to modify the membrane strain. Such a solution is interesting for some applications but makes any post patterning difficult. On the other hand, Gopalakrishnan *et al.*[13] were able to improve the flatness of Si nanomembranes by using a method called the edge-induced flattening. With a surface-energy based mechanism, they were able to reduce the distortions due to buckling. Despite its attractiveness, this approach simply enables to reduce the buckling effect, but not to fully remove it. Finally, a successful method for fabricating ultrathin silicon membranes was developed and patented in 2009 by Constancias *et al.*[5,14] This technique is based on strained SOI. Fabricating strained SOI requires several epitaxial steps.[15] Basically, it consists in growing a stack of SiGe layers on a bulk silicon wafer, in order to take advantage of the slight differences between the lattice constants of SiGe alloy and Si. First, a buffer layer is grown with a zero germanium fraction at the bottom interface, increasing to 20% at the top. A template layer of ($Si_{0.8}Ge_{0.2}$) is then grown on the buffer and followed by the epitaxial growth of a thin layer of Si on the top of it. Therefore, the thin Si layer is stretched. Afterward, the strained Si is shifted by layer transfer technic to a new handle wafer, followed by the removal of the residual SiGe layer by selective etching. The strained SOI wafers based on Si epitaxy on ($Si_{0.8}Ge_{0.2}$) show a stress of about 1.3 GPa.[16] The release process of membranes starting from strained SOI is identical to the conventional one mentioned above. The 1.3 GPa tensile stress of the Si top layer largely compensates the compressive stress of the buried oxide, leading to a buckling free silicon nanomembrane. The feasibility of this technology has already been demonstrated. However, this approach is very expensive as it involves costly technological steps and is not robust for large areas (millimeter range). Indeed, successive complex epitaxial steps are likely to cause excessive defect densities (such as misfits or threading dislocations), leading to the breakage of the membrane during manufacturing or storage.

In this work, we explore a new approach which demonstrates the fabrication of frame secured ultrathin silicon membranes using an innovative method. The fabrication process is based on the silicon direct bonding of a SOI wafer with a preperforated silicon wafer. This method prevents the buckling/ripples of the membranes by eliminating the compressive silicon oxide layer systematically present between the membrane and the frame with conventional fabrication methods. Furthermore, we applied a tensile stress to the membranes to counteract the distortions induced by their own weights (non-negligible in large areas). This method results in the fabrication of buckling free silicon nanomembranes over a large area. The membrane thickness is determined by the SOI thickness while the membrane design (size/shape) is defined by the preperforated wafer. First, in order to give the reader a comprehensive overview of our direct bonding strategy, the fabrication process based on conventional semiconductors technology is described in detail. Then we estimate the thermal differences necessary to obtain buckling free Si nanomembranes of various dimensions using analytical calculations, while the next section is devoted to the innovative direct bonding strategy. Finally, we describe practical and potential applications of such ultrathin Si nanomembranes.

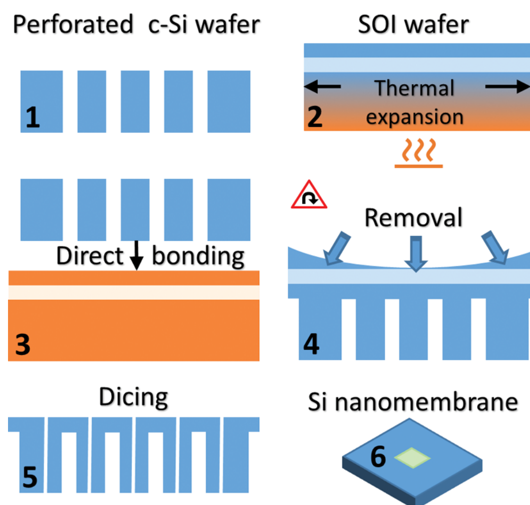

Scheme 1. Fabrication process of large area ultrathin silicon membranes by direct bonding. (1) Perforated wafer obtained with deep reactive etching; (2) pre-heating of the SOI wafer; (3) wafer bonding of a pre-perforated wafer with a pre-heated SOI wafer; (4) Si handle wafer removal and BOX etching; (5) wafer dicing; (6) single membrane secured on a frame.

RESULTS AND DISCUSSION

Fabrication Process. An innovative method for the fabrication of large area ultrathin Si membranes has been developed. It is based on the direct bonding of a SOI wafer with a preperforated silicon wafer. Scheme 1 describes the proposed approach. The first step consists in perforating the silicon wafer. The shape and size of the holes directly define the membranes design. The apertures are made by standard microtechnology approaches (hard mask, lithography, deep reactive ion etching), which enable a great flexibility in terms of shape (circular, rectangular, *etc.*) and density of the membranes.

Either epitaxial thickening or chemical etching of a standard SOI wafer are used to control the Si top layer thickness of the SOI wafer. This step determines the

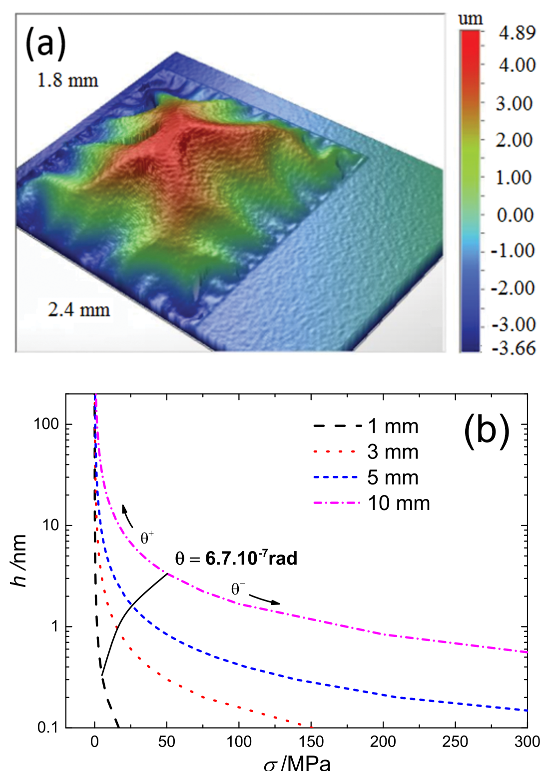

Figure 1. (a) Optical Interferometry image of the buckling of a 100 nm thick membrane made by direct SOI etching. (b) Analytical calculation of the central distortion of squared membranes with 1, 3, 5, and 10 mm sides as a function of the stress of the membrane for a thickness of 100 nm. The solid line represents the maximum deflection acceptable considering a maximum angle ($\theta = 6.7.10^{-7}$ rad) between the plane of the frame and the plane defined by the central distortion and two adjacent corners of the membrane.

membrane thickness (*e.g.*, 100 nm in our case). Then the SOI controlled wafer and the preperforated silicon wafer are put in contact to bond without any addition of external material. This technique involves silicon direct bonding.[17] Before contacting the two silicon crystals, it is necessary to prepare their surfaces chemically and physically so that they become sufficiently clean and chemically suited for direct bonding. Typically the silicon direct bonding technique involves contacting the silicon wafers at room temperature without temperature difference. The novelty of our approach is based on the use of the temperature difference between the silicon based wafers to force thermal stress during the bonding itself. Once bonded, the Si substrate of the SOI wafer is removed by mechanical grinding (diamond wheel) and wet chemical etching using the buried oxide layer as a convenient etch stop layer. Finally, the buried oxide is removed by wet etching in a standard hydrofluoric acid (HF) solution to complete the membrane release. The wafer is then ready for collective postprocessing. At this time it is possible to separate the membranes individually by wafer dicing. For that specific purpose, mechanical sawing proved to be efficient.

Theoretical Calculations. Fabricating buckling free silicon nanomembranes with conventional methods is difficult because monocrystalline Si is not obtained with a tensile stress.[18] Moreover, the selective etching of bulk Si (at nanometer scale) requires an etch stop layer (typically a silicon oxide interface). This oxide/silicon interface induces a compressive stress of several tens of MPa, which irremediably generates buckling once the membrane is released. As an example, an optical interferometer image of the buckling obtained for large area ultrathin Si membranes made by conventional method is reported in Figure 1a. A distortion of several thousands of nanometers is observed for 100 nm thick membranes with a few millimeter squared area.

In our case, the silicon oxide interface is avoided thanks to the wafer bonding approach. However, the membrane thickness is very small compared to its lateral dimensions, so that its bending stiffness is no longer sufficient to counteract the deformation induced by its weight. On the basis of the theory of plates and shells developed by Bonnotte *et al.*,[19] Constancias *et al.*[14] have recently proposed a method for determining the minimum compensation stress required to achieve a negligible deflection of a membrane with a thickness lower than one micron. An application of this method to the case of a squared monocrystalline silicon membrane with a square side results in the following equation:

$$\sigma = \frac{Pa^2}{C^*th} - \frac{E_{Si}}{1-\nu_{Si}}\frac{t^2}{C^*a^2}\left[\frac{1}{12\beta(1+\nu_{Si})} + C\frac{h^2}{t^2}\right] \quad (1)$$

with:

$$P = \rho_{Si}gt \quad (2)$$

where h is the calculated deflection, σ the stress and t the membrane thickness; g is the gravitational constant, E_{Si} the Young modulus, ν_{Si} is the Poisson's ratio and ρ_{Si} the density of silicon. As for the coefficient β, C, and C^*, they are related to form factors of the membrane and are, respectively, equal to $1.26.10^{-3}$, 26.12, and 13.63 for a squared membrane.[19] The weight is obtained assuming a pressure P uniformly applied to the membrane.

Equation 1 has been applied to our case to determine the deflection of a silicon membrane as a function of the stress of the membrane. Calculations for squared membranes with a side equal to 1, 3, and 5 mm, respectively, are reported in Figure 1b for a membrane thickness of 100 nm. The graph shows the dependence of the central distortion on the membrane stress. It is clearly seen that, for ultrathin membranes with millimeter dimensions, a tensile stress is required to avoid any distortions. For a 3 mm side square membrane (100 nm thick), a stress of 15 MPa is necessary in order to obtain a central deflection of less

TABLE 1. Estimated Stress Required To Avoid Distortion for Several Dimensions

square membrane side [mm]	minimal stress required[a] [MPa]	thermal expansion[b] $(\alpha_{Si}\Delta T) \times 10^{-5}$	ΔT^{b} [°C]
1	5	2	7
3	15	6	19
5	25	10	32
10	50	20	61

[a] Calculated from eq 1. [b] Calculated from eq 3. The thermal expansion and difference are calculated in order to obtain an equivalent strain.

than 1 nm, while the same flatness can be achieved with only a few MPa for a 1 mm^2 membrane. As the membrane side increases from 1 to 10 mm, the strain required to counteract the weight of the membrane raises considerably.

Thanks to different silicon wafer temperatures during the bonding, the thermal expansion of silicon wafers was used to force a specific thermal stress in the bonded structure. The internal stress imposed by the difference in surface temperature of the Si and the SOI wafers is determined by

$$\sigma_{\text{therm Si}} = \frac{E_{\text{Si}}}{1 - \nu_{\text{Si}}} \int \alpha_{\text{Si}}(T)\, \mathrm{d}T \qquad (3)$$

where E_{Si}, α_{Si}, and ν_{Si} are the Young modulus, the coefficient of thermal expansion (as defined by Okada *et al.*[20]), and the Poisson's ratio of silicon, respectively; dT is the thermal differential, and $\sigma_{\text{therm Si}}$ is the thermal strain.

With the mechanical model presented above, we calculated the stress required in order to obtain a 100 nm thick square membrane with a negligible distortion. For the targeted optical applications, it is more appropriate to define the maximum deflection as the maximum angle between the plane of the frame and the plane defined by the central distortion and two adjacent corners of the membrane. This angle has been determined as 6.67×10^{-7} rad, which corresponds to a maximum deflection of 1 nm with a 3 mm side membrane. These deflection values are indicated by the solid line in the Figure 1b. The corresponding stress values are related to specific differential temperatures through eq 3. The results are reported in Table 1 for different values of the square membrane side. To match the flatness requirements of our targeted applications, we estimated the thermal difference necessary to reach that minimal level of stress. For an area of 10×10 mm^2, the stress required is estimated to 50 MPa. Hence, a thermal difference of about 61 °C is required during bonding. While for a membrane of 1×1 mm^2, a stress of 5 MPa is necessary to achieve a flatness compatible with the requirements of short wavelength optics. In this case, a thermal difference of only 7 °C is theoretically sufficient during bonding.

Large Area Si Membranes by Silicon Direct Bonding. Direct bonding technique has been studied for several decades[21] resulting in successful applications.[22] However, the key point and the novelty of our process flow is the achievement of silicon direct bonding with a temperature difference. To our knowledge, it is the first time that the use of thermal difference is used in silicon direct bonding to fabricate membranes. The specific characteristics that the surfaces have to satisfy to succeed with such bonding are the following: (i) the wafers should have a controlled bow (<25 μm), (ii) an appropriate planarity (total thickness variation inferior to 10 μm), (iii) surfaces microroughness should be less than 0.3 nm RMS (root-mean-square), and (iv) surfaces have to be ultraclean (only a few particles may be present after cleaning, their diameter not exceeding 0.5 μm). In these specific conditions, silicon direct bonding can be either hydrophilic or hydrophobic. The bonding with hydrophobic approach leads to relatively weak bonding energies (20−30 mJ·m^{-2}) due to van der Waals forces between polar Si−H bonds, while it tends to be higher with a hydrophilic approach (130 mJ·m^{-2}), as the hydrogen bonds between H and O are stronger than the weak polar Si−H bonds.[17] Therefore, when an insulating ultrathin oxide layer (∼2 nm) at the bond interface is suitable, the hydrophilic method is usually preferred.

We first carried out a study on 200 mm, p-type doped Si (100) wafers in order to evaluate these two bonding strategies when a thermal difference is applied. In both cases, wet chemical cleaning was performed in order to obtain particles and contaminants free surfaces. A dynamic diluted clean based on HF was first performed to etch native or chemical oxide. For the hydrophobic approach, the surface of the wafers was then reoxidized by ozone-based chemistry as reported by Tardif *et al.*[23] Therefore, a hydrophilic surface was obtained thanks to a thin chemical SiO_2 layer. For the hydrophobic approach, in order to minimize roughness and thus increase the attractive interactions *via* van der Waals forces, a surface reconstruction generated by H_2 annealing was performed on the deoxidized Si wafers. Indeed, recent results obtained by Rauer *et al.*[24] have established that the surface reconstruction decreases the bonding interface gap, resulting in a significant increase of the bonding energies of direct hydrophobic Si bonding. Afterward, processed wafers (hydrophilic or hydrophobic) were then bonded under vacuum in an automatic bonder which enables to heat the upper and lower wafer separately prior to bonding. In our case only the lower wafer is heated. Even though the upper wafer was unintentionally heated by thermal radiation from the lower wafer (as both wafers were facing at a distance of about 5 mm in the bonder), a thermal difference occurs during the bonding process. It results in the bowing of the stacked wafers. In Figure 2b, we

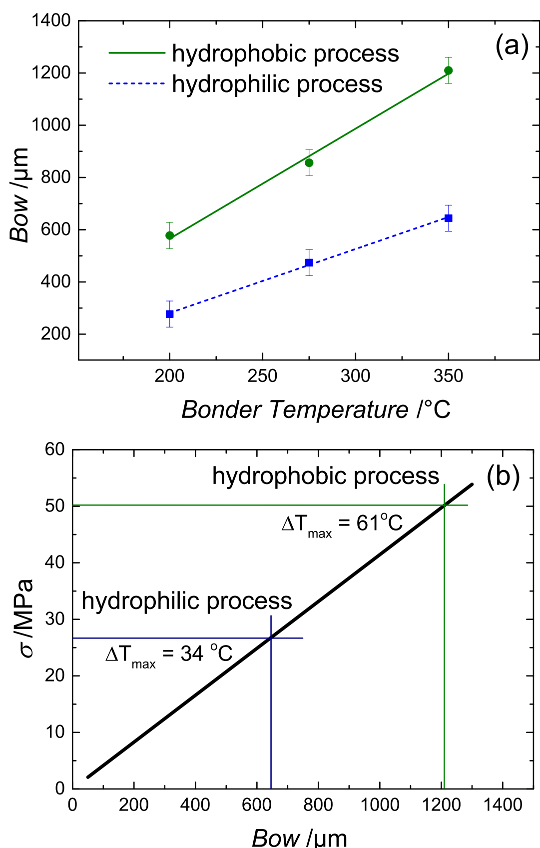

Figure 2. (a) Evolution of the bow obtained after the bonding of two Si wafers with various bonder temperatures. (b) Calculations of the stress at the bonding interface thanks to the Timoshenko formulas reported by Dunn *et al.*[25] The maximal thermal differences of each process were assessed by the calculated stress through eq 3.

report the dependence of the bow on the bonder temperature (measured at the bottom chuck) for both hydrophilic and hydrophobic bonding strategies. As the temperature was stabilized before bonding, the bonder temperature was considered equal to the temperature of the heated wafer. However, the effective thermal difference was only indirectly measurable from the bow obtained after bonding. We observe that the bow varies linearly with the bonder temperature, confirming that the process is ruled by the stress resulting from the difference in surface temperature during bonding. The maximum temperature achievable with our bonder is 350 °C. As expected, this set point allows to get the highest bow with both approaches. A maximal bow of 1210 μm was obtained with hydrophobic bonding, while a 644 μm bow was achieved with hydrophilic bonding. As the bow only results from the applied thermal difference during bonding, no difference should be observed between hydrophobic and hydrophilic strategies. However, hydrophobic bonding was performed with a preheating under vacuum of the lower wafer in the bonder, which results in a higher thermal difference during bonding. This preheating strategy was used to minimize the uncontrolled heating of the upper wafer during the thermal stabilization of the heated lower wafer. This preheating was unfortunately impossible for the hydrophilic approach as the surfaces treatments were immediately degraded by exposure to a high atmosphere at elevated temperature. It is likely that the silanol groups (Si—OH) reacted with H_2O molecules present in the atmosphere which caused the formation of an ultrathin oxide layer. This surface modification results in the decrease of the bonding energy between the wafers. Hence the bonding energy is no more sufficient to sustain the stress imposed by the thermal difference. Differently, the hydrophobic approach was able to sustain a quick atmosphere exposition up to 350 °C. Indeed the thermal budget involved is not sufficient to significantly desorb hydrogen from the surface. Hence, the hydrophobic surfaces are prevented from a sudden oxidation during the short exposure to atmosphere (required by the subsequent load of the upper wafer). The bonding energy remains sufficiently high to sustain the stress generated by the bonding process. The stress is determined by the thermal difference achieved during bonding however its value is not directly measurable. Therefore, in order to estimate it, we used the Timoshenko formulas applied to thick layers as reported by Dunn *et al.*[25] Wafer distortion analysis (followed by bow measurement) enables to determine the stress level at the interface. The bow/stress relationship in the case of two 725 μm thick wafers is shown Figure 2b. The best results for both hydrophilic and hydrophobic processes are also indicted. The hydrophilic approach enables to experimentally reach a stress of 26.7 MPa (equivalent to a thermal difference of 34 °C during bonding). The hydrophobic approach allows reaching a tensile stress of 50.1 MPa (equivalent to a thermal difference of 61 °C during bonding). These experimental results are in good agreement with the theoretical requirements reported in Table 1.

Indeed, according to the bonding results, nondeformed square nanomembranes (100 nm) with a side up to 10 mm can be achieved by the hydrophobic bonding approach as a stress of 50 MPa was achievable. Therefore, hydrophobic bonding was chosen to fabricate our membranes. However, the temperature set point with the hydrophobic bonding was voluntarily limited to 275 °C (expected bow of 882 μm), as the industrial tools used to process the bonded wafers were not secured to deal with a bow superior to 900 μm. The tensile stress, determined by this temperature set point, is expected to be 36 MPa (*cf.* Figure 2b), which is theoretically sufficient to obtain buckling free membranes up to 5 $\times$ 5 mm^2 as the thermal difference estimated during bonding is 45 °C (*cf.* Table 1). Hence, SOI and Si perforated wafers were bonded using the optimized conditions established above. The bonding process was finalized by a postbonding annealing at

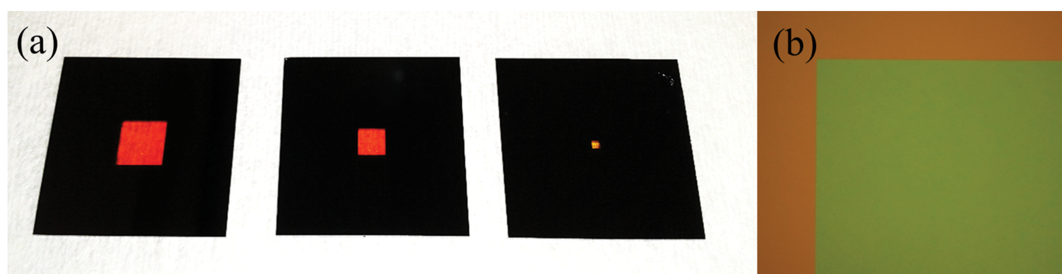

Figure 3. (a) Photography of the suspended Si nanomembranes (100 nm thick) secured on a 2 × 2 cm^2 frame (from left to right the membrane sizes are 5 × 5, 3 × 3, 1 × 1 mm^2, respectively). (b) Image of the 3 × 3 mm^2 membrane's corner from optical microscope.

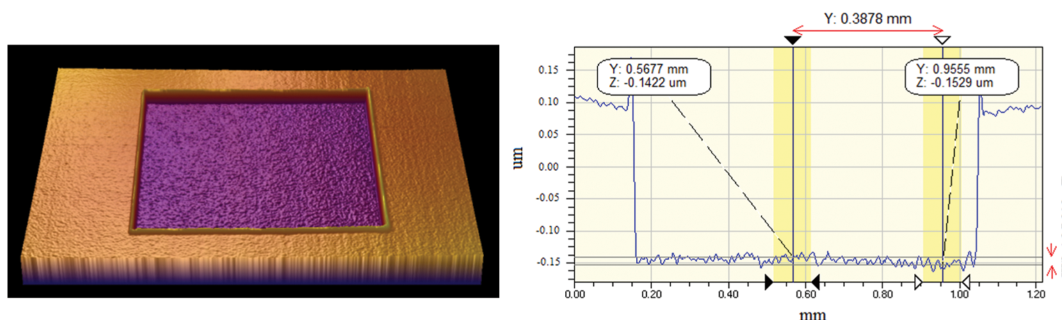

Figure 4. Optical interferometer image of the 1 × 1 mm^2 membrane and associated profile. The difference in height between the Si frame and the membrane is a measurement artifact due to the back reflection of the Si membrane. It was confirmed by SEM observation.

high temperature (1100 °C) during 2 h. After bonding, the Si handle of the SOI wafer was completely removed by chemical and mechanical polishing as detailed in the Methods section. Finally, the BOX was removed by wet etching in a diluted HF solution to complete the membrane release. Individual membranes were then separated individually by wafer dicing with a constant 2 × 2 cm^2 frame. A photograph of the resulting membranes is shown Figure 3a. One hundred nanometer thick silicon membranes of dimensions ranging from 1 × 1 up to 5 × 5 mm^2 were successfully achieved. Membrane thickness homogeneity over its whole surface was roughly verified by the color uniformity. More precisely, a silicon thickness standard deviation of 3 nm was evaluated by spectroscopic ellipsometry on the SOI wafers prior to direct bonding. Optical microscopy measurements were carried out on the membranes. A typical optical image of a 3 × 3 mm^2 membrane corner is shown Figure 3b. A perfectly defined square shape is observed and no distortions are detected. Optical interferometer images of the membranes were also carried out. The membrane flatness is well verified on the 3-dimensional view shown in Figure 4. The associated 2-dimensional profile of the membrane is also presented. We observe that the membrane flatness remains constant within approximately a 10 nm fluctuation over a 1 mm-long side dimension.

Raman scattering measurements were performed at a wavelength of 514 nm on the freestanding membranes secured to a Si frame. The spectra obtained for the membranes were compared to the spectrum of the reference silicon bulk. Application of stress is expected to cause a frequency shift toward lower wavenumbers for a tensile stress and toward higher wavenumbers for a compressive stress.[26] The experimental Raman spectra are reported in Figure 5. A distinct negative shift ($\Delta\omega$ = −0.14 cm^{-1}) of the Si related T2g mode is observed in comparison to its position in the bulk material. For (001) orientated silicon, as assuming a biaxial stress in the (100) plane, relationship between stress and Raman shift is estimated to 220 MPa·cm^{-1}.[27] The membrane stress is estimated to 31 ± 5 MPa with this linear relation. This value is in good agreement with the 36 MPa expected. The monocrystalline quality and the (001) orientation of the membrane were confirmed through electron diffraction measurements performed by transmission electron microscope (TEM). The electron diffraction pattern measured on the membrane is presented in the inset of Figure 5.

Buckling free silicon membranes (100 nm), with lateral dimensions up to 5 × 5 mm^2, were successfully achieved by hydrophobic direct bonding. Raman and optical interferometry measurements confirm the stress level and the flatness of the membranes achieved. More than 400 membranes were fabricated using this process. After complete release of the individual membranes, a fabrication yield higher than 90% was obtained. This significant value demonstrates the excellent reproducibility of this advanced fabrication process.

Applications. Critical Dimension Small Angle X-ray Scattering (CD-SAXS) has been identified as a potential solution for the measurement of sub-50 nm features.[28,29] Therefore, high resolution patterns with high aspect ratio are necessary for developing this technique and examine its sensitivity.[30] The achievement of such patterns on large area Si membranes will allow to collect high quality data in a short time in a Synchrotron facility and *in fine* to develop a laboratory Scale CD-SAXS. However, exploiting Si nanomembranes for X-rays applications requires several potential disruptive handling steps to perform nanopatterning on membrane. Even though freestanding Si nanomembranes show exceptional properties (*e.g.*, bendability),[1] they can easily break with inappropriate mechanical contact. To demonstrate the sustainability of our ultrathin Si membranes, a high resolution tungsten diffraction grating was fabricated on the membrane. First, the silicon ultrathin membrane was coated with three hundred nanometers of stress-controlled tungsten and with a very thin chromium layer using sputtering deposition. A line/space grating was then written in a thin resist layer by electron beam lithography at 100 kV (Vistec VB6 Ultra-High Resolution-Extended Wide Field). It was further transferred onto the tungsten layer *via* the consecutive etching of the chromium hard mask and the tungsten layer in an inductively coupled plasma reactor. The grating was fabricated over the whole 1 × 1 mm^2 membrane. Figure 6a. shows the scanning electron microscopy (SEM) image of the line/space grating of 50 nm half pitch achieved on the membrane. The average critical dimension measured by SEM over the membrane area shows a standard deviation smaller than 2 nm, which supports the excellent homogeneity of the processes. The successful fabrication of a high resolution diffraction grating clearly demonstrates that the Si ultrathin membrane fabricated by direct bonding are able to sustain the various demanding steps of an advanced nanofabrication necessary for X-rays optics (thin film deposition, electron beam (e-beam) lithography, plasma etching, *etc.*).[31,32] Afterward, the diffraction pattern of the 50 nm half pitch gratings was measured at the European Research Synchrotron Facility using a beamline with an energy of 17 kV and a large beam (2 mm). The measured diffraction pattern is also reported in Figure 6a. The zero-order contribution is intendedly blocked with a central beam stop. The first eight

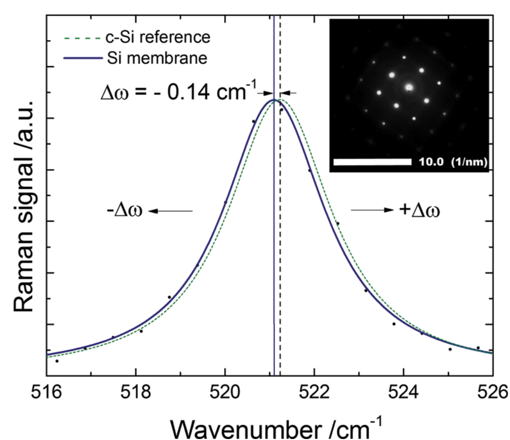

Figure 5. Raman shift measurements of a Si membrane secured on a frame. The peak is associated with the T2g Raman active mode. The dash lines show the peak position of the Si bulk reference taken on the frame. Lorentzian functions were used to fit the peaks. The inset reveals the electron diffraction pattern of the Si membrane performed on TEM. The experimental diffraction pattern in [001] zone axis directly obtained is characteristic of (100) monocrystalline Si.

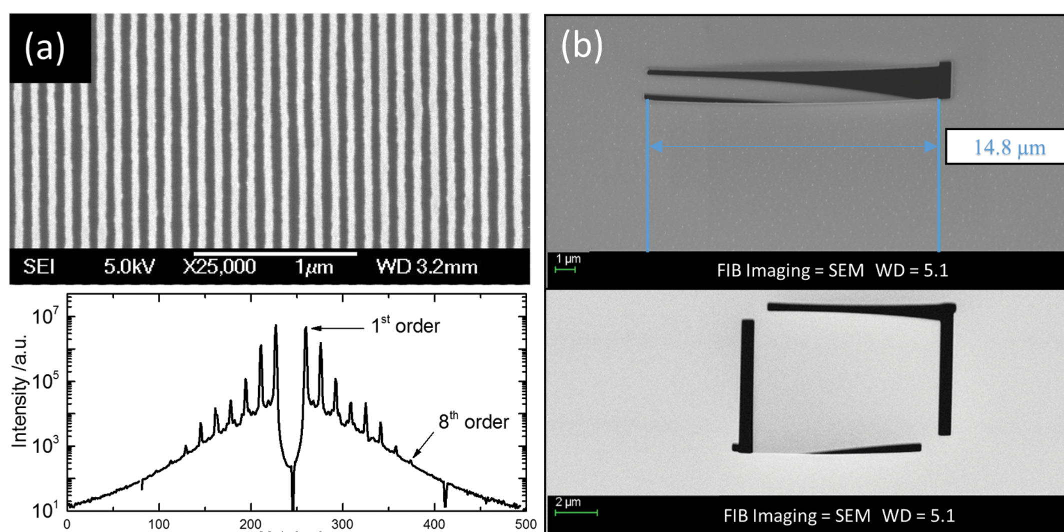

Figure 6. (a) SEM top view imaging of the 50 nm half pitch tungsten grating with an aspect ratio equal to 6 achieved on a 1 × 1 mm^2 ultrathin (100 nm) Si nanomembrane. Small angle X-ray scattering of the high resolution tungsten grating measured using synchrotron radiation at 17 keV. (b) Example of NEMS like designs achieved on a Si nanomembrane (3 × 3 mm^2) by focus ion beam (FIB). Observations were carried out using SEM tilted views.

diffraction orders of the 50 nm half pitch tungsten gratings observed on the graph are distinctively measurable. The membrane flatness and robustness under extreme illumination witness its compatibility with X-rays optics specifications. The data collected on the high resolution tungsten grating will be further used to inquire the sensitivity of the SAXS measurement to critical dimensions and other nanoscale features (*e.g.*, line edge roughness, sidewall angle, *etc.*). This work is presently in progress.

Beyond X-rays optic applications, silicon ultrathin membranes are also very attractive for the fabrication of highly sensitive sensors intended to measure displacements and extremely weak forces at the molecular scale,[33−36] or as a separation tool for biological materials.[37−39] For such applications, Si nanomembranes can be perforated to liberate nanoelectrochemical systems designs such as cantilevers or flexible structures. FIB milling was performed on a 3 × 3 mm^2 membrane. Figure 6b reports the direct observation of the ad-hoc structures carried out by SEM. The Si membranes were able to sustain important perforations in order to release a 100 nm thick NEMS-like design. The robustness of the Si nanomembranes fabricated by direct bonding is experimentally demonstrated.

CONCLUSIONS

Our results demonstrate that standard semiconductor technology can be used to fabricate large area buckling free Si nanomembranes (100 nm) by an innovative approach. Our new method, based on direct bonding with thermal difference, enables the control of the membrane thickness and the membrane design (size/shape/density) prior to bonding, which facilitates the membrane fabrication process. Hence, a wide variety of membrane designs are conceivable. Analytical calculations reported in this paper allow us to estimate the stress level necessary to avoid the membrane's distortion on a millimeter range area (up to 10 × 10 mm^2). Optimization of the direct bonding process confirms the linear thermal dependence of the stress achieved through wafer bonding. A stress of 50 MPa (estimated by the Timoshenko formulas) was experimentally achieved by hydrophobic direct bonding. Ultrathin silicon membranes (100 nm), with lateral dimensions up to 5 × 5 mm^2, were obtained by hydrophobic direct bonding. Raman, TEM and optical interferometry measurements confirmed the stress level and the flatness of the membranes achieved. The successful fabrication of a high resolution (50 nm half pitch) tungsten grating on a membrane illustrates a practical example of application for the large area ultrathin membranes performed by direct bonding with thermal difference. This accomplishment demonstrates the ability of these membranes to sustain post-fabrication nanopatterning. In addition, the quality of the diffraction pattern observed with an X-ray synchrotron source corroborates the controlled flatness achieved on these membranes, which makes them very attractive for EUV or X-ray optics fabrication (*e.g.*, diffraction gratings, Fresnel zone plates). Additional FIB millings performed on these Si nanomembranes also demonstrate their remarkable robustness. Finally, the potential of this process for ultrathin membrane fabrication is extremely promising because it is collective, applicable to other materials, and fully compatible with standard industrial semiconductor technology. Further investigations will be required to evaluate the minimal thickness (or maximal area) achievable with this process. However, preliminary results show that it is possible to fabricate 50 nm ultrathin Si membranes on 1 mm^2 with a yield higher than 90%.

METHODS

Si Ultrathin Membrane Fabrication. Two hundred millimeter (100) polished silicon wafers were perforated by standard microtechnology. An 8 μm thick silicon oxide hard mask was first deposited by plasma enhanced chemical vapor deposition (PECVD) (Applied Materials) at 240 °C on the silicon wafers. A layer of photoresist (JSR 335) was spun onto the front side of the wafers. Photolithography by ASM 100 stepper created squared window patterns (1 × 1, 3 × 3, and 5 × 5 mm^2) in the photoresist. The exposed SiO_2 was removed by RIE in an 8 in. Applied Materials P5000E using SF_6 gas. Subsequently, the etching through silicon was performed in STS ICP Etcher, allowing fast switching between the etching and the passivation steps of the "Bosch" Process. The hard mask was removed in a SMS wet bench using diluted HF etching (8%). In parallel, standard bonded SOI wafer from SOITEC, Inc. (top Si layer, 70 nm; type P BOX, 145 nm; Si handle wafer, 725 μm; details are provided in the Supporting Information) were thickened by epitaxial growing in a chemical vapor deposition reactor (RP-CVD Epi Centura) Applied Materials at 950 °C in order to adjust the Si top layer thickness of the SOI wafer. Prior to bonding, hydrophobic surface preparations were carried out on perforated and SOI wafers by means of surface reconstruction generated by the H_2 annealing at 950 °C in a RP-CVD Epi Centura, Applied Materials. Perforated and SOI wafers were then bonded in an EVG 850 bonder under vacuum atmosphere. The silicon direct bonding results in stack wafers which are then annealed at 1100 °C during 2 h under nitrogen atmosphere in a TEMPRESS horizontal furnace tube. After the bonding, the SOI handle Si side of the stack was partially grinded (600 μm) by mechanical abrasion (diamond wheel) using a DAG810 grinder DISCO and removed completely by wet chemical etching in a 12.5% TMAH solution. Membranes were separated individually by wafer dicing. For that purpose, resist from MicroChemicals (AZ4562) was spun onto the wafers (500 rpm for 30 s), followed by annealing on hot plate (80 °C for 300 s) to obtain a protective resist film thickness of several tens of micrometers that covers the membranes. Afterward the backside of the wafers were secured on a UV curable dicing tape from ADWILL (D210) prior to dicing. An automatic dicing saw from DISCO was used with a cutting speed of 3 mm/s and a water flow of 0.6 L/min, while the dicing wheel was rotated at 30 000 rpm. After dicing, the tape strong adhesion was reduced by UV irradiation to facilitate the individual pick-up of the membranes. Wet stripping by EKCLE was collectively performed on the separated dices. Finally, the BOX is removed by wet

etching in a standard 10% HF solution to complete membranes release.

Membranes Characterizations. Standard optical microscope images were obtained with an Optiphot 200 inspection microscope, Nikon. Noncontact 2D and 3D surface profile measurements were carried out with an optical profiler Veeco Wyko NT3300. Raman measurements were performed with a Renishaw system using the green light (514.5 nm) of an ion Ar laser. The spectra were recorded in triple subtractive mode with an incident laser power 0.1 mW and a 100× objective (numerical aperture of 0.9). A reference spectrum is recorded systematically, in order to eliminate any problems resulting from a frequency shift of the spectrometer. The electron diffraction measurements were performed on Titan Ultimate probe-corrected TEM at 200 kV.

Nanopatterning. Tungsten and chromium were deposited at 155 °C by sputtering on 1×1 mm^2 square Si nanomembranes using a Kurt J. Lesker. Resist from ZEON Chemicals was spun onto the individual membrane (4000 rpm for 60 s), followed by annealing on hot plate (180 °C for 300 s) to obtain a resist film thickness of 50 nm. Then a line/space grating was written by using e-beam lithography (Vistec VB6 UHR-EWF). Resist patterns were then transferred onto tungsten *via* etching in an inductively coupled plasma reactor (Plasmalab system 100 from Oxford Instrument) using consecutively chlorine and fluorine based gases. The SEM images of 50 nm half pitch grating were performed on a SEM from Jeol JSM7401F with acceleration voltage of 5 kV. Perforations of the (3×3 mm^2) Si nanomembrane were performed by MEB-FIB ZEISS NVision 40 with FIB and high-resolution field emission SEM.

Conflict of Interest: The authors declare no competing financial interest.

Acknowledgment. The authors gratefully acknowledge J.M. Hartmann for the technical assistance with the epitaxial growth. The authors would also like to thank C. Cadoux and P. Gergaud for the synchrotron radiation measurements at ESRF, D. Rouchon for the Raman measurements, E. Gautier for the MEB-FIB images, P.-H. Jouneau for the TEM measurements, S. Delprat, C. Petit Etienne and B. Dal'Zotto for their valuable contributions. This work was supported by CEA LETI, INRS and UdeM in the frame of the NanoQuébec collaborative project funding.

Supporting Information Available: Technical specifications of SOI wafers. This material is available free of charge *via* the Internet at http://pubs.acs.org.

REFERENCES AND NOTES

1. Rogers, J. A.; Lagally, M. G.; Nuzzo, R. G. Synthesis, Assembly and Applications of Semiconductor Nanomembranes. *Nature* **2011**, *477*, 45–53.
2. Kavalenka, M. N.; Striemer, C. C.; DesOrmeaux, J.-P. S.; McGrath, J. L.; Fauchet, P. M. Chemical Capacitive Sensing Using Ultrathin Flexible Nanoporous Electrodes. *Sens. Actuators, B* **2012**, *162*, 22–26.
3. Snyder, J. L.; Clark, J. A.; Fang, D. Z.; Gaborski, T. R.; Striemer, C. C.; Fauchet, P. M.; McGrath, J. L. An Experimental and Theoretical Analysis of Molecular Separations by Diffusion Through Ultrathin Nanoporous Membranes. *J. Membr. Sci.* **2011**, *369*, 119–129.
4. Gaborski, T. R.; Snyder, J. L.; Striemer, C. C.; Fang, D. Z.; Hoffman, M.; Fauchet, P. M.; McGrath, J. L. High-Performance Separation of Nanoparticles with Ultrathin Porous Nanocrystalline Silicon Membranes. *ACS Nano* **2010**, *4*, 6973–6981.
5. Constancias, C.; Dalzotto, B.; Michallon, P.; Wallace, J.; Saib, M. Fabrication of Large Area Ultrathin Silicon Membrane: Application for High Efficiency Extreme Ultraviolet Diffraction Gratings. *J. Vac. Sci. Technol., B: Nanotechnol. Microelectron.: Mater., Process., Meas., Phenom.* **2010**, *28*, 194–197.
6. Johnson, D. G.; Khire, T. S.; Lyubarskaya, Y. L.; Smith, K. J. P.; DesOrmeaux, J.-P. S.; Taylor, J. G.; Gaborski, T. R.; Shestopalov, A. A.; Striemer, C. C.; McGrath, J. L. Ultrathin Silicon Membranes for Wearable Dialysis. *Adv. Chronic Kidney Dis.* **2013**, *20*, 508–515.
7. Snyder, J. L.; Getpreecharsawas, J.; Fang, D. Z.; Gaborski, T. R.; Striemer, C. C.; Fauchet, P. M.; Borkholder, D. A.; McGrath, J. L. High-Performance, Low-Voltage Electroosmotic Pumps with Molecularly Thin Silicon Nanomembranes. *Proc. Natl. Acad. Sci. U.S.A.* **2013**, *110*, 18425–18430.
8. Iida, T.; Itoh, T.; Noguchi, D.; Takano, Y. Residual Lattice Strain in Thin Silicon-on-Insulator Bonded Wafers: Thermal Behavior and Formation Mechanisms. *J. Appl. Phys. (Melville, NY, U. S.)* **2000**, *87*, 675–681.
9. Torres, C. M. S.; Zwick, A.; Poinsotte, F.; Groenen, J.; Prunnila, M.; Ahopelto, J.; Mlayah, A.; Paillard, V. Observations of Confined Acoustic Phonons in Silicon Membranes. *Phys. Status Solidi C* **2004**, *1*, 2609–2612.
10. Shchepetov, A.; Prunnila, M.; Alzina, F.; Schneider, L.; Cuffe, J.; Jiang, H.; Kauppinen, E. I.; Sotomayor Torres, C. M.; Ahopelto, J. Ultra-Thin Free-Standing Single Crystalline Silicon Membranes with Strain Control. *Appl. Phys. Lett.* **2013**, *102*, 192108.
11. Roberts, M. M.; Klein, L. J.; Savage, D. E.; Slinker, K. A.; Friesen, M.; Celler, G.; Eriksson, M. A.; Lagally, M. G. Elastically Relaxed Free-Standing Strained-Silicon Nanomembranes. *Nat. Mater.* **2006**, *5*, 388–393.
12. Cavallo, F.; Lagally, M. G. Semiconductor Nanomembranes: A Platform for New Properties *via* Strain Engineering. *Nanoscale Res. Lett.* **2012**, *7*, 628.
13. Gopalakrishnan, G.; Czaplewski, D. A.; Mc Elhinny, K. M.; Holt, M. V.; Silva-Martínez, J. C.; Evans, P. G. Edge-Induced Flattening in the Fabrication of Ultrathin Freestanding Crystalline Silicon Sheets. *Appl. Phys. Lett.* **2013**, *102*, 033113.
14. Constancias, C.; Dalzotto, B. Method for Making a Planar Membrane. U.S. Patent 8,501,026, August 6, 2013. United States Patent and Trademark Office Web site http://patft.uspto.gov (accessed Mar 11, 2015).
15. Ghyselen, B.; Hartmann, J.-M.; Ernst, T.; Aulnette, C.; Osternaud, B.; Bogumilowicz, Y.; buckAbbadie, A.; Besson, P.; Rayssac, O.; Tiberj, A.; et al. Engineering Strained Silicon on Insulator Wafers With the Smart Cut Technology. *Solid-State Electron.* **2004**, *48*, 1285–1296.
16. Strained Silicon on Insulator. http://www.soitec.com/pdf/StrainedSOI_WP.pdf (accessed Mar 11, 2014).
17. Christiansen, S. H.; Singh, R.; Gosele, U. Wafer Direct Bonding: From Advanced Substrate Engineering to Future Applications in Micro/Nanoelectronics. *Proc. IEEE* **2006**, *94*, 2060–2106.
18. Vrinceanu, I. D.; Danyluk, S. Measurement of Residual Stress in Single Crystal Silicon Wafers. *Proc. - Int. Adv. Packag. Mater. Symp., 8th* **2002**, 297–301.
19. Bonnotte, E.; Delobelle, P.; Bornier, L.; Trolard, B.; Tribillon, G. Mise en uvre de Deux Méthodes Interférométriques pour la Caractérisation Mécanique des Films Minces par l'Essai de Gonflement. Applications au Cas du Silicium Monocristallin. *J. Phys. III* **1995**, *5*, 953–983.
20. Okada, Y.; Tokumaru, Y. Precise Determination of Lattice Parameter and Thermal Expansion Coefficient of Silicon between 300 and 1500 K. *J. Appl. Phys. (Melville, NY, U. S.)* **1984**, *56*, 314–320.
21. Gösele, U.; Tong, Q.-Y. Semiconductor Wafer Bonding. *Annu. Rev. Mater. Sci.* **1998**, *28*, 215–241.
22. Bruel, M. Silicon on Insulator Material Technology. *Electron. Lett.* **1995**, *31*, 1201–1202.
23. Tardif, F.; Lardin, T.; Maciejny, A.; Danel, A.; Boelen, P.; Cowache, C.; Kashkoush, I.; Novak, R. New Aspects of the Diluted Dynamic Clean Process. *Solid State Phenom.* **1998**, *65*, 19–22.
24. Rauer, C.; Rieutord, F.; Hartmann, J. M.; Charvet, A.-M.; Fournel, F.; Mariolle, D.; Morales, C.; Moriceau, H. Hydrophobic Direct Bonding of Silicon Reconstructed Surfaces. *Microsyst. Technol.* **2013**, *19*, 675–679.
25. Dunn, M. L.; Zhang, Y.; Bright, V. M. Deformation and Structural Stability of Layered Plate Microstructures Subjected to Thermal Loading. *J. Microelectromech. Syst.* **2002**, *11*, 372–384.

26. Wolf, I. D. Micro-Raman Spectroscopy to Study Local Mechanical Stress in Silicon Integrated Circuits. *Semicond. Sci. Technol.* **1996**, *11*, 139.
27. Anastassakis, E. Strained Superlattices and Heterostructures: Elastic Considerations. *J. Appl. Phys. (Melville, NY, U. S.)* **1990**, *68*, 4561–4568.
28. International Technology Roadmap for Semiconductors. http://www.itrs.net (accessed Mar 23, 2015).
29. Wang, C.; Jones, R. L.; Lin, E. L.; Wu, W.-L.; Rice, B. J.; Choi, K.-W.; Thompson, G.; Weigand, S. J.; Keane, D. T. Characterization of Correlated Line Edge Roughness of Nanoscale Line Gratings Using Small Angle X-Ray Scattering. *J. Appl. Phys. (Melville, NY, U. S.)* **2007**, *102*, 024901.
30. Settens, C.; Bunday, B.; Thiel, B.; Joseph Kline, R.; Sunday, D.; Wang, C.; Wu, W.-L. Critical Dimension Small Angle X-Ray Scattering Measurements of FinFET and 3D Memory Structures. *Proc. SPIE 8681* **2013**, 10.1117/12.2012019.
31. Anderson, E. H.; Olynick, D. L.; Harteneck, B.; Veklerov, E.; Denbeaux, G.; Chao, W.; Lucero, A.; Johnson, L.; Attwood, D. Nanofabrication and Diffractive Optics for High-Resolution X-Ray Applications. *J. Vac. Sci. Technol., B: Microelectron. Nanometer Struct.--Process., Meas., Phenom.* **2000**, *18*, 2970.
32. Reinspach, J.; Lindblom, M.; Bertilson, M.; Hofsten, O. V.; Hertz, H. M.; Holmberg, A. 13 nm High-Efficiency Nickel-Germanium Soft X-ray Zone Plates. *J. Vac. Sci. Technol., B: Microelectron. Nanometer Struct.—Process., Meas., Phenom.* **2011**, *29*, 011012.
33. Lavrik, N. V.; Sepaniak, M. J.; Datskos, P. G. Cantilever Transducers as a Platform for Chemical and Biological Sensors. *Rev. Sci. Instrum.* **2004**, *75*, 2229–2253.
34. Li, M.; Tang, H. X.; Roukes, M. L. Ultra-Sensitive NEMS-Based Cantilevers for Sensing, Scanned Probe and Very High-Frequency Applications. *Nat. Nanotechnol.* **2007**, *2*, 114–120.
35. Waggoner, P. S.; Craighead, H. G. Micro-and Nanomechanical Sensors for Environmental, Chemical, and Biological Detection. *Lab Chip* **2007**, *7*, 1238–1255.
36. Stowe, T. D.; Yasumura, K.; Kenny, T. W.; Botkin, D.; Wago, K.; Rugar, D. Attonewton Force Detection Using Ultrathin Silicon Cantilevers. *Appl. Phys. Lett.* **1997**, *71*, 288–290.
37. Striemer, C. C.; Gaborski, T. R.; McGrath, J. L.; Fauchet, P. M. Charge- and Size-Based Separation of Macromolecules Using Ultrathin Silicon Membranes. *Nature* **2007**, *445*, 749–753.
38. Wanunu, M.; Dadosh, T.; Ray, V.; Jin, J.; McReynolds, L.; Drndić, M. Rapid Electronic Detection of Probe-Specific MicroRNAs Using Thin Nanopore Sensors. *Nat. Nanotechnol.* **2010**, *5*, 807–814.
39. Sainiemi, L.; Viheriälä, J.; Sikanen, T.; Laukkanen, J.; Niemi, T. Nanoperforated Silicon Membranes Fabricated by UV-Nanoimprint Lithography, Deep Reactive Ion Etching and Atomic Layer Deposition. *J. Micromech. Microeng.* **2010**, *20*, 077001.